Early inner solar system origin for anomalous sulfur isotopes in differentiated protoplanets

Michael A. Antonelli[a,1,2], Sang-Tae Kim[b], Marc Peters[a], Jabrane Labidi[c], Pierre Cartigny[c], Richard J. Walker[a], James R. Lyons[d], Joost Hoek[a], and James Farquhar[a,e]

[a]Department of Geology, University of Maryland, College Park, MD 20742; [b]School of Geography and Earth Sciences, McMaster University, Hamilton, ON L8S 4K1, Canada; [c]Laboratoire de Géochimie des Isotopes Stables, Institut de Physique du Globe de Paris, UMR 7154 CNRS, Universite Paris Denis-Diderot, Sorbonne Paris Cite, 75005 Paris, France; [d]School of Earth and Space Exploration, Arizona State University, Tempe, AZ 85287; and [e]Earth System Science Interdisciplinary Center, University of Maryland, College Park, MD 20742

Edited by Mark H. Thiemens, University of California, San Diego, La Jolla, CA, and approved November 5, 2014 (received for review September 30, 2014)

Achondrite meteorites have anomalous enrichments in ^{33}S, relative to chondrites, which have been attributed to photochemistry in the solar nebula. However, the putative photochemical reactions remain elusive, and predicted accompanying ^{33}S depletions have not previously been found, which could indicate an erroneous assumption regarding the origins of the ^{33}S anomalies, or of the bulk solar system S-isotope composition. Here, we report well-resolved anomalous ^{33}S depletions in IIIF iron meteorites (<−0.02 per mil), and ^{33}S enrichments in other magmatic iron meteorite groups. The ^{33}S depletions support the idea that differentiated planetesimals inherited sulfur that was photochemically derived from gases in the early inner solar system (<~2 AU), and that bulk inner solar system S-isotope composition was chondritic (consistent with IAB iron meteorites, Earth, Moon, and Mars). The range of mass-independent sulfur isotope compositions may reflect spatial or temporal changes influenced by photochemical processes. A tentative correlation between S isotopes and Hf-W core segregation ages suggests that the two systems may be influenced by common factors, such as nebular location and volatile content.

iron meteorites | sulfur isotopes | protoplanetary disk | solar system | photochemistry

Of all of the extraterrestrial materials found on Earth, iron meteorites have always been the most conspicuous. So-called "magmatic" iron meteorites are likely to be samples from the cores of magmatically differentiated protoplanetary parent bodies (1), whereas "nonmagmatic" iron meteorites are commonly suggested to sample solidified melt pockets that formed via impacts onto nondifferentiated (chondritic) parent bodies (2). Individual members from an iron meteorite group are assumed to derive from a common parent body, based on shared chemical and isotopic characteristics (1–4). Chemical and isotopic differences among the different iron groups provide convincing evidence that different individual parent body planetesimals incorporated genetically distinct precursor materials (1–4).

Recent observations that several achondrite meteorite groups possess small, mass-independent ^{33}S enrichments relative to chondrites (5) have led to the conclusion that sulfur isotopes were heterogeneously distributed among the materials that accreted to form early solar system planetesimals. This observation, coupled with the ancient ^{182}Hf-^{182}W ages (within 1–3 My of solar system formation) of magmatic irons (6–8), provides impetus to search for systematic variations in mass-independent sulfur isotope compositions among the iron groups.

Results

We report high-precision $\delta^{34}S$, $\Delta^{33}S$, and $\Delta^{36}S$ data (where $\Delta^{33}S = 1000 \times \{\delta^{33}S - [(\delta^{34}S + 1)^{0.515} - 1]\}$ and $\Delta^{36}S = 1000 \times \{\delta^{36}S - [(\delta^{34}S + 1)^{1.9} - 1]\}$) for 61 troilite (FeS) nodules extracted from 58 different iron meteorites selected from eight different groups (IAB, IC, IIAB, IIE, IIIAB, IIIF, IVA, and IVB) (Fig. 1, Fig. S1, and Tables S1 and S2). All groups except for IAB and IIE have been classified as magmatic (1, 2). Our data for group IAB includes five chemically (and possibly genetically) distinct subgroups (2). Collectively, all of the iron meteorites examined have overlapping $\delta^{34}S$ values consistent with those reported by previous studies (9, 10), ranging from −1.41‰ to +1.29‰ with an average of −0.01 ± 0.81‰ (2σ SD, 2s.d.) (Fig. 1). We have chosen to report uncertainties either as 2σ SEs (2SE) where appropriate (for averages derived from groups with more than eight analyzed members), or as 2s.d. long-term external reproducibility for individual data points and for groups where the number of analyzed samples is small (±0.3‰, ±0.008‰, and ±0.3‰ for $\delta^{34}S$, $\Delta^{33}S$, and $\Delta^{36}S$, respectively; see *SI Text*, Fig. S2, and Tables S3 and S4). There is no distinction between magmatic and nonmagmatic irons in $\delta^{34}S$, and most individual groups have average $\delta^{34}S$ values within 2s.d. of zero (±0.3‰).

In contrast to $\delta^{34}S$, the new results show that $\Delta^{33}S$ values are uniform within iron meteorite groups, but that there are resolvable $\Delta^{33}S$ differences between different groups. Values of $\Delta^{33}S$ range from −0.031‰ to +0.031‰ [normalized to troilite from the Canyon Diablo IAB iron meteorite (CDT)], with different iron meteorite groups forming discernible clusters in $\Delta^{33}S$ space (Fig. 1). The nonmagmatic iron meteorites examined show a limited range in $\Delta^{33}S$ compared with magmatic irons: Group IAB ($n = 23$), including samples from the main group (including CDT), three subgroups, two grouplets, and several ungrouped IAB iron meteorites, has an average $\Delta^{33}S$ of +0.004 ± 0.002‰

Significance

This investigation focuses on the sulfur isotopic compositions of magmatically differentiated meteorites, the oldest igneous rocks in our solar system. We present evidence of anomalous ^{33}S depletions in a group of differentiated iron meteorites, along with ^{33}S enrichments in several other groups. The complementary positive and negative compositions, along with observed covariations in ^{36}S and ^{33}S, are explained by Lyman-α photolysis of gaseous H_2S in the solar nebula. Confirmation of photochemically predicted ^{33}S depletions implies that the starting composition of inner solar system sulfur was chondritic, consistent with the Earth, Moon, Mars, and nonmagmatic iron meteorites. Differentiated protoplanets, however, appear to have accreted from materials processed under conditions where sulfur was volatile and UV radiation was present (<~2 AU).

Author contributions: M.A.A. and J.F. designed research; M.A.A., S.-T.K., M.P., J.L., J.H., and J.F. performed research; M.A.A., S.-T.K., M.P., J.L., P.C., R.J.W., J.R.L., and J.F. analyzed data; and M.A.A., P.C., R.J.W., J.R.L., and J.F. wrote the paper.

The authors declare no conflict of interest.

This article is a PNAS Direct Submission.

[1]To whom correspondence should be addressed. Email: mantonelli@berkeley.edu.

[2]Present address: Department of Earth and Planetary Science, University of California, Berkeley, CA 94720.

This article contains supporting information online at www.pnas.org/lookup/suppl/doi:10.1073/pnas.1418907111/-/DCSupplemental.

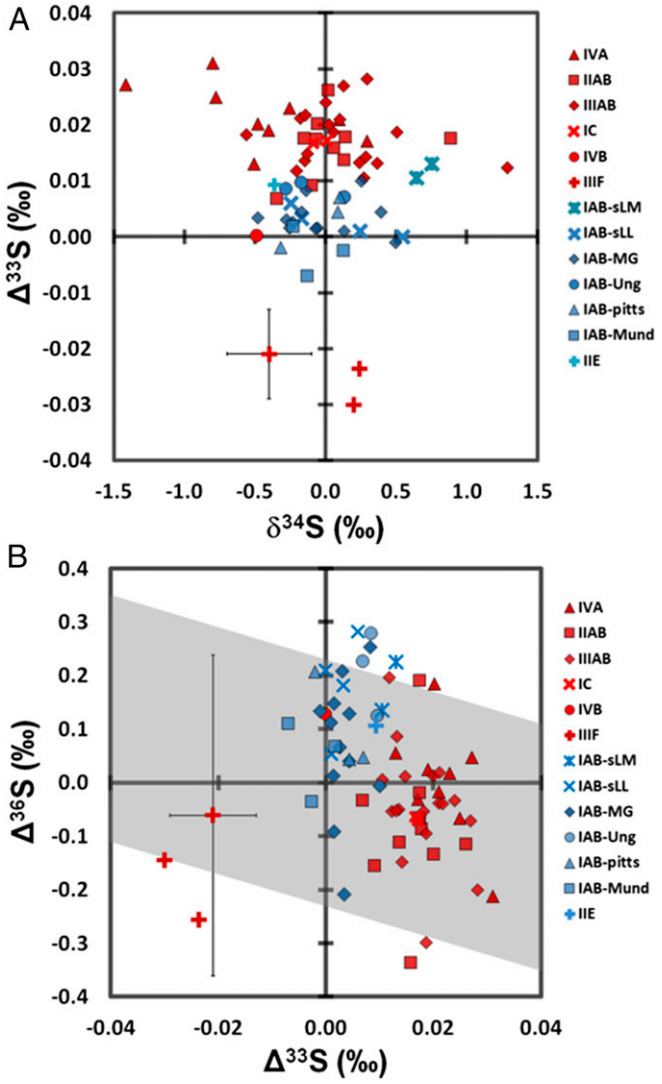

Fig. 1. Sulfur isotope measurements in iron meteorite troilite. Measurements of (*A*) $\Delta^{33}S$ vs. $\delta^{34}S$ and (*B*) $\Delta^{36}S$ vs. $\Delta^{33}S$, for acid-volatile sulfur fractions (n = 72) of troilite from 58 iron meteorites belonging to the groups IAB, IC, IIAB, IIE, IIIAB, IIIF, IVA, and IVB. Nonmagmatic and magmatic groups are in blue and red, respectively. Error bars, shown on a single point, represent 2s.d. uncertainties of 0.3‰, 0.008‰, and 0.3‰ for $\delta^{34}S$, $\Delta^{33}S$, and $\Delta^{36}S$, respectively. Gray band demarcates the fractionation array of H_2S ($\Delta^{36}S/\Delta^{33}S$ of ∼−3) by Ly-α photolysis (27). One additional S-isotope measurement on group IIIF (10) is also included.

(2SE), while Watson, the single meteorite analyzed from nonmagmatic group IIE, has a $\Delta^{33}S$ of +0.010 ± 0.008‰ (2s.d.). Members analyzed from the IAB subgroups do not have resolvable mass-independent sulfur isotopic differences compared with the main group (Fig. 1 and Table S2); this observation is consistent with, but does not require, their derivation from a single parent body (2).

Magmatic irons are characterized by mass-independent S-isotope compositions resolvable from zero (Table S2). Groups IIAB, IIIAB, and IVA have means and 2SE errors, +0.016 ± 0.004‰, +0.018 ± 0.002‰, and +0.022 ± 0.004‰, respectively. Group IC has a mean $\Delta^{33}S$ of +0.017‰, while the only sample analyzed from group IVB has a $\Delta^{33}S$ of 0.000‰; magmatic group IIIF is characterized by an average negative $\Delta^{33}S$ of −0.027‰ [in these cases, the number of analyzed samples is small; uncertainty is comparable to or less than long-term external reproducibility (2s.d. = ±0.008‰)].

Average $\Delta^{36}S$ measurements within their uncertainties, like those for $\delta^{34}S$, also overlap for most iron meteorite groups, ranging from −0.34‰ to +0.28‰ (Fig. 1*B*). However, the nonmagmatic irons appear to have slightly positive $\Delta^{36}S$, while the magmatic irons tend to have more negative values. Two-tailed heteroscedastic t tests were performed between groups to probe the statistical significance of our $\Delta^{36}S$ isotope measurements (Table S5). These tests demarcate the probability that two sets of measurements come from the same population, with the output variable (the P value) representing the fractional probability that the two sets are identical. When comparing the $\Delta^{36}S$ of magmatic groups IIAB, IIIAB, and IVA to group IAB, P values returned were lower than ∼0.02, indicating a >98% chance that they represent different populations. Although the relationship is poorly defined, there appears to be a negative correlation between $\Delta^{36}S$ and $\Delta^{33}S$ [$\Delta^{36}S/\Delta^{33}S \sim -7 \pm 4$ (2s.d.)] that is similar to that calculated from available bulk achondrite analyses (5) [$\Delta^{36}S/\Delta^{33}S \sim -6 \pm 6$ (2s.d.)] (Fig. S3).

Fractionation Mechanisms That Affect $\Delta^{33}S$. While a number of mechanisms exist that can fractionate sulfur isotopes, only a few are known to produce the types of variations in $\Delta^{33}S$ and $\Delta^{36}S$ seen in our data, and many others can be ruled out. For instance, magmatic processes produce small-magnitude, mass-dependent fractionations because they occur at high temperature and are associated with equilibrium isotope partitioning. Furthermore, kinetic processes that could potentially generate larger fractionations do not provide a simple explanation for the variations of $\Delta^{33}S$ and $\Delta^{36}S$, considering the small range of observed $\delta^{34}S$. Recent studies of magnetic isotope effects (11) have demonstrated that $\Delta^{33}S$ can be modified by processes related to interactions between nuclear and electronic spin of radical intermediates; however, these effects do not produce variations for $\Delta^{36}S$ and are not considered to be viable candidates to account for our observations. Another recent study regarding fractionation of gases in imposed low-temperature thermal gradients (of ∼100 °C) has also demonstrated the existence of small anomalous isotope effects capable of modifying $\Delta^{33}S$ (12), but the authors could not resolve an effect for $\Delta^{36}S$. Below, we discuss several mechanisms that have been shown to produce small variations of $\Delta^{33}S$ related to mixing, distillation, and evaporation, and evaluate whether they can explain the iron meteorite data.

Mixing of sulfur pools with different mass-dependent S-isotopic compositions yields small deviations from the mass-dependent array—referred to as mass conservation effects (13). Considering that the largest $\delta^{34}S$ variations found in carbonaceous chondrite sulfides are ±8‰ (14), mixing could only generate a $\Delta^{33}S$ of +0.008‰. Given that the range of $\delta^{34}S$ found in iron meteorites is significantly smaller, only a very small $\Delta^{33}S$ (+0.001‰) is anticipated as a result of mixing processes, making mixing unlikely as an explanation for the observed variation.

Rayleigh distillation is another type of mass conservation effect that involves the extraction of sulfur from a reactant to produce product and residue with isotopic compositions that lie above the original mass fractionation line (slightly positive $\Delta^{33}S$). McEwing et al. (15) performed an experiment for which they evaporated troilite at low pressure and high temperature. Measuring $\delta^{34}S$, they determined the fractionation factors associated with the branched reaction for evaporation of troilite to elemental sulfur ($1000\ln\alpha = -13$‰) and to dissociated troilite ($1000\ln\alpha = -5.4$‰). Using their data and assuming canonical mass-dependent fractionation, the $\Delta^{33}S$ variations due to mixing between products and reactants during Rayleigh distillation of troilite to elemental sulfur was calculated to yield a maximum $\Delta^{33}S$ of ∼ +0.009‰ (Fig. S4), decreasing as the reaction's branching ratio increases toward dissociated troilite. However, the minor sulfur isotopes were not measured, and it is possible that this process deviates slightly from the canonical value; moreover, a recent

experimental study (16) has documented anomalous mass laws associated with low-temperature condensation and evaporation of SF_6. The authors (16) attributed this effect to a competition between low-frequency vibrational modes associated with weak chemical interactions between SF_6 clusters in the condensed phase and high-frequency modes associated with the stronger S–F bonds in the clusters themselves and in the free gas-phase SF_6. They diagramed the principle of this competition between effects that enrich the heavy isotope with a shallow slope (e.g., 0.505) and effects that enrich the light isotope with a steeper slope (e.g., 0.515).

To explore whether this may apply to troilite evaporation (which does not have discrete individual S clusters like SF_6), we consider how the contributions from modes that enrich the heavy isotope and those that enrich the light isotope are related to temperature. Inferring a dependence on $h\nu/kT$, we project that the contributions from both modes will decrease as temperature increases, reducing the magnitude of the anomalous isotope effect. Direct experiments to evaluate the mass dependence of troilite evaporation are needed to resolve this conclusively, but several other lines of evidence exist to suggest that troilite evaporation does not produce a large anomalous effect, including the following. (*i*) studies of the isotope effects for sulfur associated with impact gardening of mature lunar soils have been interpreted to indicate that impact devolatilization of sulfur can produce large variations for $\delta^{34}S$, but these processes have canonical mass-dependent fractionations (17). (*ii*) Data for $\Delta^{33}S$ and $\Delta^{36}S$ in the main group of IAB iron meteorites and IAB subgroups (presented here), which are suggested to have been formed by various impacts on a chondritic parent body (2), reveal no resolvable anomalous sulfur isotopic variability. (*iii*) Isotopic measurements of lunar basalts (this study and ref. 18) exhibit $\Delta^{33}S$ and $\Delta^{36}S$ that are not distinguishable from the terrestrial mantle (19), which suggests that the putative Moon-forming giant impact (and subsequent basin-forming impacts) did not fractionate sulfur isotopes in a mass-independent fashion. These three lines of evidence suggest that impact and evaporation processes did not produce the variation seen among the different iron meteorite groups.

Nucleosynthetic and Cosmogenic Production of Rare Sulfur Isotopes. Cosmic ray effects could also potentially be responsible for the small observed variations in $\Delta^{33}S$ and $\Delta^{36}S$ in iron meteorites. In previous studies of spallogenic sulfur production from Fe in the metal phase of iron meteorites, a positive correlation between cosmic ray exposure proxies and both $\Delta^{33}S$ and $\Delta^{36}S$ was observed (9, 10) [$\Delta^{36}S/\Delta^{33}S \sim +8$]. Iron meteorites from many of the groups analyzed in this study (such as the IAB irons) span a large range of cosmic ray exposure ages (20), yet there is no correlation between exposure age proxies (neutron fluence) and the sulfur isotopic composition of troilite. Spallogenic sulfur in the metal phase of iron meteorites is generated from target Fe atoms and found at parts per million concentrations. However, troilite contains a lower concentration of target Fe atoms and a much higher concentration of autochthonous sulfur atoms (10^4 times higher than observed in the metal phase). Additionally, the slope of the relation obtained for $\Delta^{36}S/\Delta^{33}S$ [$\sim -7 \pm 4$ (2s.d.)], although poorly constrained, is opposite to that predicted for the spallogenic production of sulfur from Fe [($\Delta^{36}S/\Delta^{33}S \sim +8$) (9, 10)]. Instead, the resolvable mass-independent sulfur isotopic differences between magmatic iron groups indicate that different parent bodies likely formed from genetically distinct precursor materials, consistent with evidence from other isotopic systems (1, 3, 4).

Nucleosynthetic anomalies in S would most likely be found through measurements of $\Delta^{36}S$ (21) because the nucleosynthetic pathways for ^{32}S, ^{33}S, and ^{34}S are related in stellar environments (22, 23). In comparison, ^{36}S, the rarest and therefore the most sensitive of the four stable sulfur isotopes, is created in unique conditions within massive stars before Type II supernova explosion (24). However, recent measurements of presolar SiC by secondary ion mass spectrometry have identified several grains with large ^{32}S excesses (25). We have modeled the effect of injection of a pure ^{32}S component into the early solar nebula on the $\Delta^{33}S$ and $\Delta^{36}S$ compositions of bulk solar system materials and find that this leads to a unidirectional departure from CDT composition with a $\Delta^{36}S/\Delta^{33}S$ slope of −1.9 about the origin (Fig. S4), which does not overlap with the iron meteorite array ($\sim -7 \pm 4$). Furthermore, addition of ^{32}S can only lead to negative $\Delta^{33}S$ values, and leaves the (most abundant) positive $\Delta^{33}S$ signatures unexplained, unless the starting composition of bulk solar system was highly positive ($>+0.161‰$).

The rare stellar regions that have been suggested to possibly produce positive $\Delta^{33}S$ (excess ^{33}S) are modeled to produce even greater volumes of excess ^{36}S (24), which have not been documented in presolar grains or at the bulk scale. Additionally, small nucleosynthetic anomalies described for other elements in iron meteorites [such as molybdenum (4)], do not correlate with our sulfur isotope measurements, which would likely be expected if they were attributable to the same mechanism. The injection of sulfur from any nucleosynthetic source would produce a unidirectional departure from CDT, which could only explain our observations if the bulk initial $\Delta^{33}S$ composition of the solar system was nonchondritic, and if the concentration of sulfur in presolar grains was not negligible relative to the total sulfur budgets of early-forming planetesimals.

Fractionation Mechanisms Associated with Gas-Phase Photochemistry. Photochemically driven isotope fractionation, on the other hand, could have produced anomalous sulfur with both positive and negative $\Delta^{33}S$ and $\Delta^{36}S$ variations from a reservoir of bulk chondritic composition. Predictions for sulfur isotope behavior during photochemical reactions, however, rely on a very limited number of experimental studies undertaken at relevant conditions. Photolysis of H_2S by UV radiation with wavelengths longer than ∼220 nm (26) yields a positive $\Delta^{36}S/\Delta^{33}S$ array ($\sim +1.7$) which does not match our observations. A series of recent photolysis experiments on H_2S using Lyman-α (Ly-α) radiation, however, provide a possible match to the observed sulfur isotope compositions in iron meteorites, with an array between products and reactants delineating a $\Delta^{36}S/\Delta^{33}S$ ratio of ~ -3 (27). Given our uncertainties on $\Delta^{36}S$ and the limited spread of our data, this array supports a preaccretionary photochemical origin for the S-isotope signatures seen in troilite from magmatic irons (Fig. 1*B*). Of the currently known anomalous fractionations, it is Ly-α photolysis of H_2S (27) that is most consistent with the negative correlation between $\Delta^{36}S$ and $\Delta^{33}S$ observed in both iron and achondrite meteorites (Fig. S3) and with the conditions present in the inner solar system.

Feasibility of a Photochemical Origin. Hydrogen sulfide, the most abundant sulfur-bearing gas in the early solar system, is suggested to have resided within the inner ∼2 AU of the young solar nebula (28, 29), and near the surfaces of the disk, because temperatures exceeded ∼700 K, resulting in the evaporation of troilite. Ly-α radiation from the Sun would have been highest during the T-Tauri phase of solar history, which lasts ∼2 My for a star of solar mass (30). A calculation that takes into account the Far-UV photon flux (at 1 AU) for a T-Tauri star of solar mass, and the penetration depth of Ly-α radiation into an evolving protoplanetary disk, presented below, demonstrates that $\Delta^{33}S$ signals of the magnitude observed could be produced, on relevant timescales, in the young protoplanetary disk (see *SI Text* for details).

To model H_2S photolysis, we use the evolving solar nebula model of Hersant et al. (31) [the same used in Pasek et al. (28)], which has time-dependent midplane temperature and disk

Table 1. Disk model parameters and time required to photolyze 2% of nebular H_2S for high-mass and low-mass disks with solar and subsolar H_2O abundances

Disk type	T_0, K	Σ_0, g cm^{-2}	H, AU	$n_H(0)$, cm^{-3}	C/O ratio	Z_{ph}, AU	$t_\nu(Z_{ph})$, y	$n_H(Z_{ph})/n_H(0)$	$N_{overturns}$ (2% photolysis)	Time required, y
High-mass	1050	5000	0.064	8.6×10^{14}	solar	0.288	320	4.0×10^{-5}	500	1.6×10^5
(t <50 Ky)	—	—	—	—	~1.5	0.28	310	7.0×10^{-5}	285	8.8×10^4
Low-mass	700	650	0.052	1.4×10^{14}	Solar	0.21	200	2.9×10^{-4}	70	1.4×10^4
(t <500 Ky)	—	—	—	—	~1.5	0.202	180	5.3×10^{-4}	40	7.2×10^3

T_0, the midplane temperature; Σ_0, the surface density at midplane; H, the scale height; n_H, the number density of H atoms at midplane; Z_{ph}, the penetration limit (height above midplane) of Ly-α radiation; $t_\nu(Z_{ph})$, the time required for one overturn at height Z_{ph}; $n_H(Z_{ph})/n_H(0)$, the ratio of H atoms at Z_{ph} over the midplane value; $N_{overturns}$, the number of overturns required.

surface density, but we assume an isothermal vertical temperature profile, implicitly adding viscous heating (Table 1). The depth of penetration of stellar UV radiation into the solar nebula is determined primarily by dust absorption. The low angle of incidence, and the predominantly forward-scattering nature of the dust, implies strong absorption of stellar UV in the nebular surface region of the disk. By contrast, stellar Ly-α radiation interacts with the H atom layer in the uppermost regions of the nebula, and resonant scattering from H atoms redirects a portion of the Ly-α photons on trajectories more perpendicular to the disk midplane (32). To determine the depth of penetration of Ly-α into the disk at different times in nebular history, we computed the total optical depths from H_2O, H_2S, and dust: the main absorbers of Ly-α radiation (Table S6).

Assuming solar elemental abundances (33) and a fraction of O atoms trapped in SiO_3 bonds (pyroxene dust) (31), we calculated the Ly-α optical depths for all three absorbers considered here at several values of Z for two end member scenarios, an early high-mass disk (<5×10^4 y) and a late low-mass disk (<5×10^5 y) (Table S6). For the cases with reduced water abundance, [C/O = 1.5], H_2S photolysis will occur slightly deeper in the disk. A more refined calculation (*SI Text*) for penetration depth takes into account the photolysis timescale for an H_2S molecule at different depths, and yields the depth at which this does not exceed the timescale for turbulent mixing (Table 1), which is in agreement with our coarser estimates.

The depth of penetration for Ly-α photons can be used to estimate the time needed to photolyze a given fraction of the H_2S present in the nebula. The iron meteorites measured here have a maximum $\Delta^{33}S$ of ~0.03‰ in troilite grains. H_2S photolysis experiments using Ly-α (27) yielded a maximum fractionation of $\Delta^{33}S$ ~1.5‰ in elemental sulfur, suggesting that only ~2% of total disk H_2S was photolyzed and trapped in the region of the nebula where magmatic iron meteorite parent body materials were produced. Assuming that turbulent vertical mixing was present due to a magnetorotational instability at 1 AU, the overturn rates are ~200–300 y (Table 1).

For the two protoplanetary disks of different mass, we calculate the number of overturns necessary to photolyze 2% of total H_2S at 1 AU and find that the timescales for potential production of the anomalous $\Delta^{33}S$ signal are less than 200 Ky (Table 1), consistent with the early accretion and core segregation ages of differentiated protoplanets (1, 6–8).

Additional to the anomalous sulfur produced by H_2S photolysis, other photochemical production mechanisms involving exotic sulfur species [e.g., SiS, HS, AlS, and/or PS (28)] may have also taken place, but photolysis experiments involving these high-temperature sulfide gases have not yet been performed. Despite this fact, we show that photolysis of H_2S is sufficient to explain both the covariation and magnitude of our data on the necessary timescales.

Implications for Accretion of Differentiated Protoplanets. Trapping photolytic sulfur into a secondary, distinct, chemical phase(s) is required to preserve and transfer an anomalous $\Delta^{33}S$ signal to the precursor materials of magmatic iron parent bodies. However, mechanisms through which these isotope signatures were incorporated into protoplanets remain poorly understood. Due to the higher condensation temperatures of refractory sulfides, such as oldhamite (CaS) [(~1,200 K) (28)], compared with silicates, their condensation likely occurred within a region optically clear to UV radiation from the young sun. However, the condensation temperature of troilite (~700 K) is inferior to that of most silicates (28), making it likely that it condensed at higher optical depths. We suggest that the most parsimonious mechanism for incorporation of photolytic sulfur isotope signatures into solid grains is through their incorporation into refractory sulfides such as oldhamite (which can condense in optically thin regions of the solar nebula). The largest positive $\Delta^{33}S$ deviation in achondrites is for oldhamite from the Norton County aubrite (5). Aubrites are thought to come from a highly reduced planetesimal parent body, which is likely to have formed in the innermost regions of the disk (34). Refractory sulfides (such as oldhamite) thus could have acted as early transient carriers of anomalous sulfur into differentiated planetesimal parent bodies in the inner solar system.

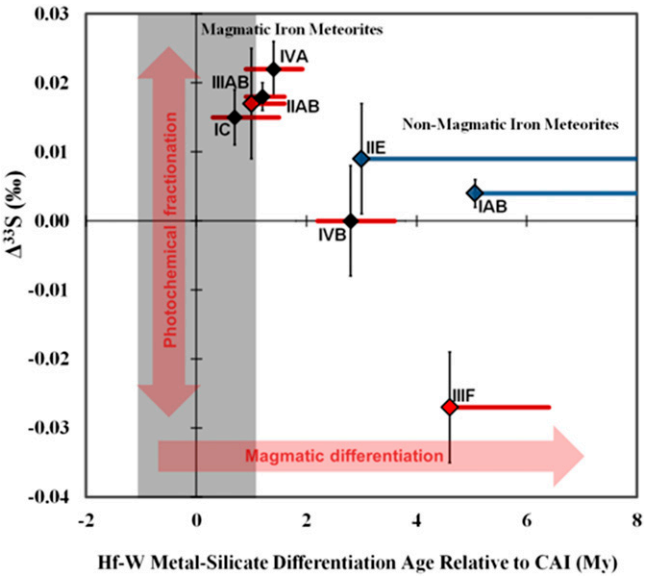

Fig. 2. $\Delta^{33}S$ vs. exposure-corrected Hf-W metal-silicate segregation ages. Average $\Delta^{33}S$ for each group of magmatic (red) (n = 6) and nonmagmatic (blue) (n = 2) iron meteorites plotted against Hf-W ages. Solid black diamonds represent preexposure $\varepsilon^{182}W$ values (6), hollow diamonds represent maximum calculated cosmogenic exposure corrections on groups IC and IIIF (8), and Sm-based corrections on IAB and IIE (7). Colored lines span the range of maximum corrected values from available data. Error bars represent 2SE for IAB, IVA, IIAB, & IIIAB, and 2s.d. (±0.008‰) for other groups. Gray band represents uncertainty in calcium-aluminum inclusion (CAI) initial.

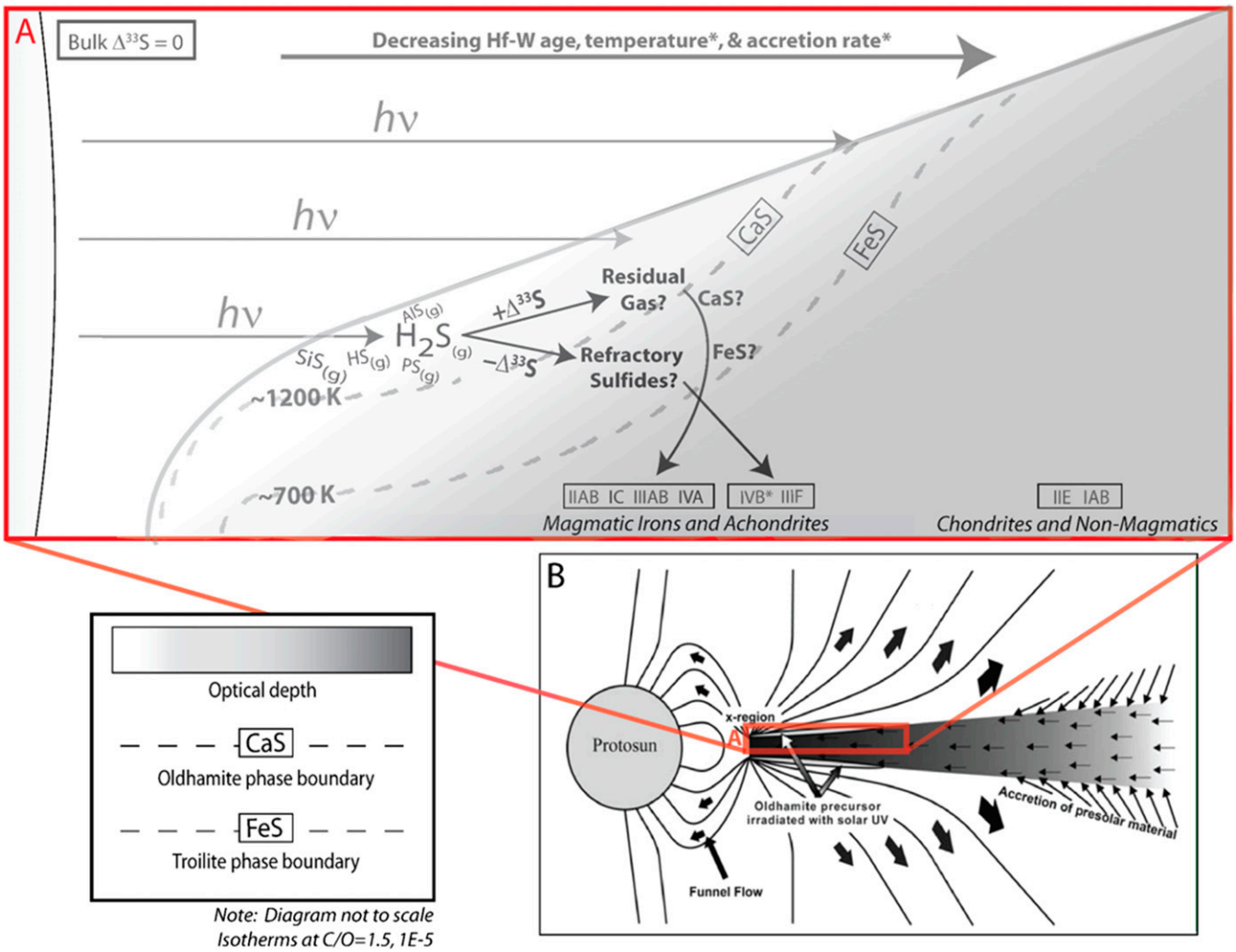

Fig. 3. (*A*) Proposed model for sulfur isotope distribution in early solar nebula. In this working model, Hf-W age, temperature, and accretion rate roughly decrease to the right with increasing heliocentric distance. Anomalous $\Delta^{33}S$ is created through the photolysis of sulfur-bearing gases and captured in refractory sulfides that settle down to the midplane, joining other precursors for iron meteorite and achondrite parent bodies. The paucity of H_2S and greater optical depth inhibit the generation of anomalous sulfur signatures at greater heliocentric distances. Isotherm temperatures are from ref. 28. (*B*) The solar nebula during T-Tauri phase, showing the formation zone of the oldhamite precursor suggested to have carried anomalous sulfur to achondrites . Adapted from ref. 5 with permission from AAAS.

Magmatic iron meteorites progress from positive $\Delta^{33}S$ to negative $\Delta^{33}S$ values, corresponding weakly with published Hf-W core segregation ages (6–8) (Fig. 2). This may be linked to a process associated with the timing or location of the accreting parent bodies. A recent study (6) suggests that the different core segregation ages of magmatic iron parent bodies may be controlled significantly by the volatile content of the accreting materials. An unrelated study has recently suggested that low-volatile materials accreted first in the solar nebula, due to their higher densities (35); if the Hf-W differentiation ages are also related to volatile contents, the relationship between Hf-W age and $\Delta^{33}S$ may represent the gradual removal of an anomalous refractory S component from an inner solar system reservoir. However, the IIIF iron meteorites do not fit the volatile vs. Hf-W age correlation, and $\Delta^{33}S$ values do not appear to correlate with published volatile data in a straightforward fashion, which implies that the correlation between $\Delta^{33}S$ and Hf-W age is not simply a matter of volatile abundance. Other factors, such as the accretion age and nebular location of the different parent bodies, are likely to have also influenced their different core segregation ages and $\Delta^{33}S$ values. Nonmagmatic irons (including IAB subgroups) have $\Delta^{33}S$ indistinguishable from bulk chondrites and Hf-W segregation ages several million years later than most magmatic irons (6–8). Such iron meteorites do not preserve evidence for inheritance of a photochemical sulfur component, and may have accreted in more distal parts of the solar nebula with greater optical densities and at ambient temperatures that precluded the presence of gas-phase H_2S.

The heliocentric region suggested to have once contained sulfur-bearing gases available for photolysis in the early solar system (28, 29) (<~2 AU) has also been suggested (through dynamical arguments) as the birthplace of differentiated meteorite parent bodies (36). Combining these constraints with those provided by our sulfur isotope measurements, a working model emerges that links the photolysis of gas-phase sulfur species by Ly-α radiation to the distribution of mass-independent sulfur isotope signatures that were captured by early-forming, inner solar system planetesimals (Fig. 3). The sulfur isotope data suggest that magmatic iron and achondrite parent bodies formed in regions proximal to the Sun, where high temperatures and high photon fluence enabled the creation of anomalous sulfur isotope signatures through gas-phase photolysis. The similar negative $\Delta^{36}S/\Delta^{33}S$ arrays

for achondrites and iron meteorites is consistent with a shared genetic heritage, and may provide a new system for linking iron groups to their rocky counterparts.

Our new data suggest potential links between the inner solar system and planetesimals with internal heat sources sufficient for early magmatic differentiation. The $\Delta^{33}S$ (and $\Delta^{36}S$) values of the Earth, Moon, and Mars, which are indistinguishable from IAB iron meteorites/bulk chondrites (18, 19, 37, 38), are intermediate between the ^{33}S-enriched and ^{33}S-depleted isotopic compositions observed in magmatic irons and achondrites. This implies that the complementary photolytic sulfur isotope signatures captured by these early-formed differentiated protoplanets were either diluted by the later addition of materials with isotopically normal (chondritic/IAB) sulfur or were recombined during the continued accretionary processes that formed the terrestrial planets.

Materials and Methods

Acid volatile sulfur was obtained from crushed troilite nodule samples (~3–10 mg) allowing the measurement of sulfur isotopic ratios in monosulfide minerals. The samples were heated with degassed 5 N HCl bubbled with flowing N_2 gas; the released H_2S (dominantly from troilite) was then passed through condensers, through an acid trap containing ultrapure water, and captured in a slightly acidic trapping solution containing $AgNO_3$. The precipitated Ag_2S was thoroughly rinsed with ultrapure water and 1 M NH_4OH solution before drying. This Ag_2S was then reacted with *ca.* 10 times stoichiometric excess of pure F_2 in Ni fluorination bombs at 250 °C overnight, producing SF_6 gas which was subsequently purified with cryogenic and gas chromatographic techniques. The sulfur isotope abundances were measured using a ThermoFinnigan MAT 253 mass spectrometer monitoring *m/z* = 127, 128, 129, and 131 ($^{32}SF_5^+$, $^{33}SF_5^+$, $^{34}SF_5^+$, and $^{36}SF_5^+$). All results are reported in per mil (‰) relative to CDT using standard delta notation $\delta^iS = 1000 \times \{[(^iS/^{32}S)_{sample}/(^iS/^{32}S)_{CDT}] - 1\}$, where i = 33, 34, 36.

ACKNOWLEDGMENTS. We thank T. J. McCoy, T. Mittal, L. Nittler, J. T. Wasson, B. A. Wing, and anonymous reviewers for useful advice and comments, and L. Welzenbach for help obtaining samples. M.A.A. acknowledges NSERC postgraduate scholarship funding (PGS-M-420592- 2012) that aided in supporting this work. J.F. acknowledges NASA Cosmochemistry Grants NNX09AF72G and NNX13AL13G. R.J.W. acknowledges NASA Cosmochemistry Grant NNX13AF83G.

1. Benedix GK, Haack H, McCoy TJ (2014) Iron and stony-iron meteorites. *Meteorites, Comets, and Planets,* Treatise on Geochemistry, eds Herzog GF, Gibson EK, Jr (Elsevier, Amsterdam), Vol 1, pp 41–61.
2. Wasson JT, Kallemeyn GW (2002) The IAB iron-meteorite complex: A group, five subgroups, numerous grouplets, closely related, mainly formed by crystal segregation in rapidly cooling melts. *Geochim Cosmochim Acta* 66(13):2445–2473.
3. Clayton RN, Mayeda TK, Olsen EJ, Prinz M (1983) Oxygen isotope relationships in iron meteorites. *Earth Planet Sci Lett* 65(2):229–232.
4. Burkhardt C, et al. (2011) Molybdenum isotope anomalies in meteorites: Constraints on solar nebula evolution and origin of the Earth. *Earth Planet Sci Lett* 312(3):390–400.
5. Rai VK, Jackson TL, Thiemens MH (2005) Photochemical mass-independent sulfur isotopes in achondritic meteorites. *Science* 309(5737):1062–1065.
6. Kruijer TS, et al. (2014) Protracted core formation and rapid accretion of protoplanets. *Science* 344(6188):1150–1154.
7. Schulz T, Upadhyay D, Munker C, Mezger K (2012) Formation and exposure history of non-magmatic iron meteorites and winonaites: Clues from Sm and W isotopes. *Geochim Cosmochim Acta* 85:200–212.
8. Qin L, Dauphas N, Wadhwa M, Masarik J, Janney PE (2008) Rapid accretion and differentiation of iron meteorite parent bodies inferred from ^{182}Hf- ^{182}W chronometry and thermal modeling. *Earth Planet Sci Lett* 273(1-2):94–104.
9. Hulston JR, Thode HG (1965) Cosmic-ray produced ^{36}S and ^{33}S in metallic phase of iron meteorites. *J Geophys Res* 70(18):4435–4442.
10. Gao X, Thiemens MH (1991) Systematic study of sulfur isotopic composition in iron meteorites and the occurrence of excess ^{33}S and ^{36}S. *Geochim Cosmochim Acta* 55(9): 2671–2679.
11. Oduro H, Van Alstyne KL, Farquhar J (2012) Sulfur isotope variability of oceanic DMSP generation and its contributions to marine biogenic sulfur emissions. *Proc Natl Acad Sci USA* 109(23):9012–9016.
12. Sun T, Bao H (2011) Thermal-gradient-induced non-mass-dependent isotope fractionation. *Rapid Commun Mass Spectrom* 25(6):765–773.
13. Farquhar J, Johnston DT, Wing BA (2007) Implications of conservation of mass effects on mass-dependent isotope fractionations: Influence of network structure on sulfur isotope phase space of dissimilatory sulfate reduction. *Geochim Cosmochim Acta* 71(24):5862–5875.
14. Bullock ES, McKeegan KD, Gounelle M, Grady MM, Russel SS (2010) Sulfur isotopic composition of Fe-Ni sulfide grains in CI and CM carbonaceous chondrites. *Met Planet Sci* 45(5):885–898.
15. McEwing CE, Thode HG, Rees CE (1980) Sulphur isotope effects in the dissociation and evaporation of troilite: A possible mechanism for ^{34}S enrichment in lunar soils. *Geochim Cosmochim Acta* 44:565–571.
16. Eiler J, Cartigny P, Hofmann AE, Piasecki A (2013) Non-canonical mass laws in equilibrium isotopic fractionations: Evidence from the vapor pressure isotope effect of SF_6. *Geochim Cosmochim Acta* 107:205–219.
17. Thode HG, Rees CE (1979) Sulphur isotopes in lunar and meteorite samples. *Lunar Planet Sci* 10:1629–1636.
18. Wing BA, Farquhar J (2014) Planetary sulfur isotopic baseline from lunar basalts. *Geochim Cosmochim Acta*, in press.
19. Labidi J, Cartigny P, Moreira M (2013) Non-chondritic sulphur isotope composition of the terrestrial mantle. *Nature* 501(7466):208–211.
20. Eugster O, Herzog GF, Marti K, Caffee MW (2006) Irradiation records, cosmic-ray exposure ages, and transfer times of meteorites. *Meteorites and the Early Solar System II*, eds Lauretta DS, McSween HY (Univ Arizona Press, Tucson, AZ), pp 829–851.
21. Clayton DD, Ramadurai S (1977) On presolar meteoritic sulfides. *Nature* 265(5593): 427–428.
22. Chin YN, Henkel C, Whiteoak JB, Langer N, Churchwell EB (1996) Interstellar sulfur isotopes and stellar oxygen burning. *Astron Astrophys* 305:960–969.
23. Heger A, Woosley SE, Rauscher T, Hoffman RD, Boyes MM (2002) Massive star evolution: Nucleosynthesis and nuclear reaction rate uncertainties. *New Astron Rev* 46(8-10):463–468.
24. Woosley SE, Heger A (2007) Nucleosynthesis and remnants in massive stars of solar metallicity. *Phys Rep* 442(1-6):269–283.
25. Fujiya W, Hoppe P, Zinner E, Pignatari M, Herwig F (2013) Evidence for radiogenic sulfur-32 in type AB presolar silicon carbide grains? *Astrophys J* 776:L29.
26. Farquhar J, Savarino J, Jackson TL, Thiemens MH (2000) Evidence of atmospheric sulphur in the martian regolith from sulphur isotopes in meteorites. *Nature* 404(6773):50–52.
27. Chakraborty S, Jackson TL, Ahmed M, Thiemens MH (2013) Sulfur isotopic fractionation in vacuum UV photodissociation of hydrogen sulfide and its potential relevance to meteorite analysis. *Proc Natl Acad Sci USA* 110(44):17650–17655.
28. Pasek MA, et al. (2005) Sulfur chemistry with time-varying oxygen abundance during solar system formation. *Icarus* 175(1):1–14.
29. Ciesla FJ (2013) Sulfidization of iron in a dynamic solar nebula and the implications for planetary compositions. *Lunar Planet Sci Conf* 44:1315.
30. Wolk SJ, et al. (2005) Stellar activity on the young suns of Orion COUP observations of K5-7 pre-main-sequence stars. *Astrophys J* (suppl 160):1–49.
31. Hersant F, Gautier D, Hure J-M (2001) A two-dimensional turbulent model for the solar nebula constrained by D/H measurements in the solar system: Implications for the formation of giant planets. *Astrophys J* 554:391–407.
32. Bethell TJ, Bergin EA (2011) The propagation of Ly-α in evolving protoplanetary disks. *Astrophys J* 739(2):78.
33. Asplund M, Grevesse N, Sauval AJ, Scott P (2009) The chemical composition of the Sun. *Annu Rev Astron Astrophys* 47:481–522.
34. Keil K (2010) Enstatite achondrite meteorites (aubrites) and the histories of their asteroidal parent bodies. *Chem Erde* 70(4):295–317.
35. Hubbard A, Ebel DS (2014) Protoplanetary dust porosity and FU Orionis outbursts: Solving the mystery of Earth's missing volatiles. *Icarus* 237:84–96.
36. Bottke WF, Nesvorný D, Grimm RE, Morbidelli A, O'Brien DP (2006) Iron meteorites as remnants of planetesimals formed in the terrestrial planet region. *Nature* 439(7078): 821–824.
37. Franz HB, et al. (2014) Isotopic links between atmospheric chemistry and the deep sulphur cycle on Mars. *Nature* 508(7496):364–368.
38. Rai VK, Thiemens MH (2007) Mass-independently fractionated sulfur components in chondrites. *Geochim Cosmochim Acta* 71(5):1341–1354.